

## COAL ANALYSIS BY TG-FTIR

P.R. Solomon, M.A. Serio, R.M. Carangelo, and R. Bassilakis  
Advanced Fuel Research, Inc.  
87 Church Street, East Hartford, CT 06108 USA

**KEYWORDS:** Coal, Analysis, Pyrolysis, Combustion, TGA, FTIR

### INTRODUCTION

Thermogravimetric analysis has been employed in coal science to perform a number of characterizations including: proximate analysis (1), kinetics of weight loss (2,3) char reactivity (4-9) and gas adsorption measurements (10). A complimentary technique, evolved product analysis, has been employed to study pyrolysis product distributions and kinetics (11-18) functional group compositions (14,19-21), and temperature programmed desorption (22-24).

We have developed a TG-FTIR instrument which combines thermogravimetric analysis (TGA) with evolved product analysis by Fourier Transform Infrared (FT-IR) spectroscopy. FT-IR analysis of evolved products has advantages over mass spectroscopy in allowing analysis of very heavy products, and over gas chromatography in speed. To analyze coal, a sequence of drying, pyrolysis and combustion is employed to obtain: proximate analysis, volatiles composition, volatiles kinetics, and relative char reactivity. The application of TG-FTIR to coal and petroleum source rock has recently been described (25,26). The purpose of this paper is to describe the most recent improvements in the apparatus.

### EXPERIMENTAL

**Apparatus** - A schematic of the instrument is presented in Fig. 1. Its components are as follows: a DuPont™ 951 TGA; a hardware interface (including a furnace power supply); an Infrared Analysis 16 pass gas cell with transfer optics; a MICHELSON 110 FT-IR; (Resolution: 4  $\text{cm}^{-1}$ , Detector: MCT). A helium sweep gas is employed to bring evolved products from the TGA directly into the gas cell. This instrument package is now available commercially as the TG/plus from Bomem, Inc.

The most difficult volatiles to analyze are the heavy decomposition products which condense at room temperature, such as tars from coal. In the TG/plus, the high conductivity helium sweep gas and the rapid cooling causes these products to form an aerosol which is fine enough to follow the gas through the analysis cell. The cell is connected without restrictions to the sample area. The aerosol is also fine enough that there is little scattering of the infrared beam and it is thus attenuated as though the tar was in the gas phase.

**Procedure** - As an example of the analysis procedure, the pyrolysis and oxidation of a lignite is described. More detail can be found in Refs. 25 and 26. Figure 2a illustrates the weight loss from this sample and the temperature history. A 35 mg sample of Indian Head Zap lignite, loaded in the sample basket of the DuPont™ 951, is taken on a 30°C/min temperature excursion in the helium sweep gas, first to 150°C where it is held for 4 minutes to dry, then to 900°C for pyrolysis. The temperature is held at 900°C for 3 minutes. After cooling to 250°C, a small flow of  $\text{O}_2$  is added to the furnace at the 57 minute mark and the temperature is ramped at 30°C/min to 700°C (or higher) for oxidation.

During this excursion, infrared spectra are obtained once every thirty seconds. As discussed previously (25,26), the spectra show absorption bands for  $\text{CO}$ ,  $\text{CO}_2$ ,  $\text{CH}_4$ ,  $\text{H}_2\text{O}$ ,  $\text{SO}_2$ ,  $\text{COS}$ ,  $\text{C}_2\text{H}_4$ , olefins,  $\text{HCl}$ , and  $\text{NH}_3$ . The spectra above 400°C also show aliphatic, aromatic, hydroxyl, carbonyl and ether bands from tar. The evolution of gases derived from the IR absorbance spectra are obtained by a quantitative analysis program which employs a database of integration regions and calibration spectra for different compounds. The routine decides which regions of each calibration spectrum to use for best quantitation with the least interferences. The routine is fast so the product analysis is displayed during the actual experiment.

Figure 2b illustrates the integral of the evolution curves to obtain cumulative evolved product amounts. Because the data are quantitative, the sum of these curves match the weight loss as

determined by the TGA balance. Discrepancies occur in this match because of missing components such as  $H_2$  which cannot be seen by IR and  $H_2S$  which is very difficult to see. Secondly, when  $O_2$  is introduced, the balance shows a net gain in weight due to  $O_2$  chemisorption.

**Calibration** - To calibrate the instrument, known flows for calibration gases were mixed with a fixed flow of sweep gas and passed through the gas cell. Reference spectra were collected and the flow rate was varied to provide spectra over the range of expected concentrations. The quantitative analysis program employs the spectrum which most closely matches the experimental amplitudes since Beer's law (absorption is proportional to concentration) is not valid for many light gases.

Calibration spectra cannot be employed in the same way for tar since the absorptivity of any band varies with the tar compositions. Instead, the evolution of tar is derived by using the spectrum of a Pittsburgh Seam coal tar as a calibration standard. This coal tar has all the functional group features (but at different intensities) characteristic of coal tars. Its use as a reference spectrum determines the important tar functional group regions whose amplitudes provide a qualitative tar evolution profile for other coals. The tar's evolution determined in this manner typically exhibits a sharply peaked function with increasing temperature as shown in Fig. 3a.

To quantitatively determine the tar loss, it is assumed that the qualitative tar evolution profile is proportional to the rate of loss of tar. This will be true when the functional group compositions of the tar does not change with temperature, a condition which holds over most of the tar evolution profile as indicated by examining the infrared spectra at various times during its evolution. To determine the constant of proportionality for each sample, the tar loss profile is compared to the rate of weight loss from the balance minus the rate of weight loss for all the gases. This quantity is presented in Fig. 3b. The proportionality constant is picked by performing a least squares fit between the two curves over the region of tar evolution, except for parts where other gases are evolving quickly and might introduce error. The proportionality constant varies systematically from 0.86 times the absorptivity for Pittsburgh Seam coal for Zap lignite to 1.56 times Pittsburgh Seam coal for Pocahontas in agreement with the lower absorptivity of the aromatic components in the higher rank coals.

Routine calibration of the instrument is performed on a monthly basis using calcium oxalate. A typical evolution profile is presented in Fig. 4. The calcium oxalate has three weight loss regions yielding  $H_2O$ ,  $CO_2$ , and  $CO$ . The agreement between the sum of gases and weight loss shows that the calibration and the sweep gas flow rate are accurate. The positions of peaks compared to a known reference validates the accuracy of the thermocouple temperature measurement. To check for possible leaks in the system and the absence of oxygen in the helium sweep gas, graphite is run periodically. If there are no leaks and the helium is of high purity, no appreciable weight loss or  $CO_2$  evolution is experienced during the pyrolysis cycle.

**Samples** - The coals analyzed were Argonne premium coal samples. The characterization of these samples has appeared elsewhere (27). In addition, demineralized coals were produced using the technique of Bishop and Ward (28). This technique removes both discrete minerals as well as organically bound alkali or alkaline earth metals. Oxidized samples were prepared in an oven at  $100^\circ C$  or at room temperature in air.

## RESULTS AND DISCUSSION

**Analysis of Argonne Coals** - Analyses were performed for eight Argonne coals at both  $3^\circ C/min$  and  $30^\circ C/min$ . Results for three coals for the pyrolysis cycle ( $30^\circ C/min$ ) are presented in Figs. 5 to 7. Figures 5a to 7a presents the weight losses and temperature profiles. Also presented (dashed line) is the sum of species (tar,  $CH_4$ ,  $H_2O$ ,  $CO_2$ ,  $CO$ ,  $SO_2$ , and  $NH_3$ ). In general, the sum of species is within a few percent of the weight loss.

The evolution of tar and aliphatic gases is presented in Figs. 5c to 7c. These tar evolution profiles typically consist of a low temperature peak or shoulder followed by a narrow larger peak. The low temperature peak is believed to be due to the evaporation of unattached "guest" molecules (the molecular phase). The higher temperature peak is due to the release of coal fragments by bond breaking, evaporation and transport (29). In Fig. 5c, these peaks are labeled 1 (molecular phase) and 2 (pyrolysis).

Methane evolution is presented in Figs. 5e to 7e. Methane evolution occurs in two closely spaced peaks. The low temperature peak is initiated coincident with the initiation of tar evolution, but reaches a maximum at a slightly higher temperature than the maximum tar peak. The temperature for the maximum evolution varies little with rank but the temperature of initiation of methane evolution decreases with decreasing rank. The second peak appears as a shoulder on the high temperature side of the first peak. In Fig. 5e, these peaks are labeled 1 (methane loose) and 2 (methane tight).

Water evolution is presented in Figs. 5b to 7b. Water appears first at low temperature when the coal's moisture is evolved. For all coals, a prominent water peak also occurs simultaneously with the tar peak. This suggests that the chemistry responsible for this peak is either related to the free radicals produced, or the increase in fluidity (and hence mobility for bi-molecular interactions), both of which occur during tar formation. Burnham et al. (17) report the coincidence of the tar peak with the low temperature peaks for  $\text{CO}_2$  and  $\text{H}_2\text{S}$ , which supports the idea that tar evolution is associated with the decomposition of heteroatom functionalities. There is also a higher temperature  $\text{H}_2\text{O}$  peak and a lower temperature peak or shoulder accompanying  $\text{CO}_2$  evolution in low rank coals. In Fig. 7b, these peaks are labeled 1 (moisture), 2 (water extra loose, associated with early  $\text{CO}_2$  evolution), 3 (water loose, associated with tar evolution), and 4 (water tight).

Figures 5d to 7d present the results for  $\text{CO}_2$ . Wyodak (Fig. 7d) which is typical of low rank coals, shows three peaks between 200 and 900°C labeled 2 (extra loose associated with  $\text{H}_2\text{O}$ ), 3 (loose associated with tar evolution and  $\text{H}_2\text{O}$  evolution) and 4 ( $\text{CO}_2$  tight). There is also a very low temperature peak labeled 1 (occurring only for the lowest rank coals) whose origin is presently unknown. Higher rank coals usually have peaks 3 and 4 but not peak 2 unless they are oxidized. Peak 2 is one of the regions affected most by oxidation. In addition, the evolution of  $\text{CO}_2$  is often complicated in high rank coals by the evolution of  $\text{CO}_2$  from carbonates such as calcite (Fig. 6d) and siderite.

The evolution of CO is presented in Figs. 5f to 7f. Low rank coals exhibit three peaks labeled 3, 4, and 5 as shown in Fig. 7f. Peaks 3 and 4 coincides with the  $\text{CO}_2$  peaks 3 and 4, while peak 5 has no accompanying peaks for  $\text{H}_2\text{O}$  or  $\text{CO}_2$ . CO peaks also can be seen accompanying the  $\text{CO}_2$  calcite peak (see Fig. 6). High rank coals appear to have only the high temperature peak 5.

Results for other gases are presented in parts g to i of Figs. 5 to 7. The  $\text{C}_2\text{H}_2$  yield shown in Figs. 5g to 7g occurs in a narrow evolution peak which lags the tar peak but precedes the methane. The ammonia evolution in Fig. 5h to 7h appear to coincide with the start of CO evolution (Figs. 5f to 7f). The  $\text{SO}_2$  peak near 28 minutes (Figs. 5i to 7i) appears to coincide with one of the COS peaks (Figs. 5j to 7j).

Sample results for the combustion cycle are presented in Fig. 8. Since oxygen is added, the reported weight loss is for the elements C, H, S, not the oxide. This will make the sum of the elements (C, H, and S) lost less than the total measured weight loss, the difference being the oxygen in the char. The combustion cycle is dominated by the evolution of  $\text{CO}_2$ , CO, and  $\text{SO}_2$ . The sum of the C, H, and S in these species is in reasonable agreement with the weight loss.

**Analysis of Minerals** - The identification of evolution peaks due to minerals was made by performing TG/plus analysis of reference minerals and demineralized coals. An important contributor is calcite. The major reaction is the evolution of  $\text{CO}_2$  near 800°C. There are also small amounts of CO and  $\text{H}_2\text{O}$  evolved. The  $\text{CO}_2$  peak is almost identical in shape and position to that exhibited by the Illinois No. 6 coal in Fig. 6e. When the Illinois coal was demineralized (dashed line) the 800°C  $\text{CO}_2$  peak disappears. The demineralized coal also shows a small increase in the tar yield and little moisture, but no other major changes.

Several high rank coals (Pocahontas, Upper Freeport, and Pittsburgh) showed  $\text{CO}_2$  peaks at about 525°C which disappeared with demineralization. The 520°C peak appears to be due to siderite based on the discussion by Raask (30).

**Volatile Kinetics** - The TG-FTIR analysis can be used to study product evolution kinetics. We have compared in Fig. 19, the temperature for the maximum hydrocarbon evolution rate for the Argonne coals as a function of rank at 0.05 and 0.5°C/sec. Duplicate runs were all within  $\pm 4^\circ\text{C}$ . The peak temperatures as well as the shape of the tar peaks are in good agreement with the results of

Burnham et al. obtained using a Rock-Eval analyzer (17) and a Triple-Quadrupole Mass Spectrometer (TQMS). The 50 to 65°C shift in temperatures with heating rate corresponds to activation energies approximately between 45 and 60 Kcal/mole. The variation in the rate of thermal decomposition is in part responsible for the variation of ignition behavior with rank (31).

**Functional Group Composition** - The TG-FTIR analysis provides information on the coal's functional group composition since it is the functional group composition which gives rise to the variation in gas yields. Figure 9b shows the variation in oxygen containing products with rank. Low rank coals have a high content of oxygen functional groups.

Figure 9c presents the data for tar and CH<sub>4</sub> yields. Methane increases systematically with increasing rank. High volatile bituminous coals have the most tar. Tar yields are related to soot formation in combustion (31) to fluidity (32), and to yields in liquefaction (33) or mild gasification (34). The tar functional group composition can also be obtained from the infrared spectra during tar evolution.

**Char Properties** - The TG-FTIR analysis provides two measurements related to char reactivity. The first is the weight gain of the char which occurs when oxygen is added early in the combustion cycle (see Fig. 2b). This weight gain is proportional to the concentration of active sites which are accessible to O<sub>2</sub>. The second measurement is of the temperature required to produce a specified rate of weight loss during the oxidation cycle. As discussed previously, this critical temperature T<sub>cr</sub> is related to the reactivity (4-7). The higher the reactivity, the lower T<sub>cr</sub>.

Figure 9d compares both the oxygen chemisorbed and T<sub>cr</sub> as functions of the oxygen in the coal. There is a systematic decrease in T<sub>cr</sub> and an increase in oxygen chemisorbed with increasing oxygen. The interplay of decomposition kinetics and reactivity control the ignition behavior and burnout in combustion or gasification (31).

## CONCLUSIONS

A single TG-FTIR analysis provides an extensive coal characterization with regard to the decomposition kinetics, char reactivity, functional group compositions and conversion behavior.

## ACKNOWLEDGEMENT

Work was supported by the U.S. Department of Energy, Morgantown Energy Technology Center under Contract No. DE-AC21-86MC23075 and under NSF SBIR Grant No. ISI-8703520.

## REFERENCES

1. Ottaway, M., *Fuel*, **61**, 713-716, (1982).
2. Ciuryla, V.T., Weimer, R.F., Bivans, A., and Motika, S.A., *Fuel*, **58**, 748, (1979).
3. van Krevelen, D.W., van Heerden, C., and Huntjens, F.J., *Fuel*, **30**, 253, (1951).
4. Solomon, P.R., Serio, M.A., and Heninger, S.G., *ACS Div. of Fuel Chem. Preprints*, **31**, (3), 200-209, (1986).
5. Best, P.E., Solomon, P.R., Serio, M.A., Suuberg, E.M., Mott, W.R, Jr., and Bassilakis, R., *ACS Div. of Fuel Chem. Preprints*, **32**, (4), 138-146, (1987).
6. Serio, M.A., Solomon, P.R., Bassilakis, R., and Suuberg, E.M., *ACS Div. of Fuel Chem. Preprints*, **34**, (1), 9-21, (1989).
7. Serio, M.A., Solomon, P.R., Bassilakis, R., and Suuberg, E.M., The Effects of Minerals on Coal Reactivity, Int. Conf. on Coal Science, Japan, (10/89).
8. Jenkins, R.G., Nandi, S.P., and Walker, P.L., Jr., *Fuel*, **52**, 288, (1973).
9. Sahu, R., Levendis, Y.A., Flagan, R.C., and Gavalas, G.R., *Fuel*, **67**, 275-283, (1988).
10. Suuberg, E.M., Calo, J.M., and Wojtowicz, W., *ACS Div. of Fuel Chem. Preprints*, **31**, (3), 186-193, (1986).
11. Juntgen, H. and van Heek, K.H., *Fuel Proc. Tech.*, **2**, 261, (1979).
12. Winans, R.E., McBeth, R.L., and Neill, P.H., *ACS Div. of Fuel Chem. Preprints*, **33**, (3), 85-90, (1988).
13. Chakravarty, T., Windig, W., Hill, G.R., and Meuzelaar, H.L.C., *Energy & Fuels*, **2**, (4), 400-405, (1988).
14. Solomon, P.R. and Hamblen, D.G., Finding Order in Coal Pyrolysis Kinetics, Topical Report

- submitted to U.S. Department of Energy under Contract No. DE-AC21-FE05122, 1983, also *Progress in Energy and Combustion Science*, **9**, 323-361, (1983).
15. Fitzgerald, D. and van Krevelen, D.W., *Fuel*, **38**, 17, (1959).
  16. Campbell, J.H., *Fuel*, **57**, 217, (1978).
  17. Burnham, A.K., Oh, M.S., Crawford, R.W., and Samoun, A.M., *Energy & Fuels*, **3**, (1), 42-55, (1989).
  18. Weimer, R.F. and Ngan, D.Y., *ACS Div. of Fuel Chem. Preprints*, **24**, (3), 129-140, (1979).
  19. Attar, A. and Dupuis, F., *ACS Div. of Fuel Chem. Preprints*, **23**, (2), 44-53, (1978).
  20. Attar, A. and Hendrickson, G.G., *Coal Structure*, (R.A. Meyers, Ed.), Academic Press, NY, Chapter 5, p. 131, (1982).
  21. LaCount, R.B., Anderson, R.R., Friedman, S., and Blaustein, B.D., *Fuel*, **66**, 909-913, (1987).
  22. Hall, P.J. and Calo, J.M., *Energy & Fuels*, **3**, (3), 370-376, (1989).
  23. Zhang, Z.G., Kyotani, T., and Tomita, A., *Energy & Fuels*, **3**, 566-571, (1989).
  24. Kyotani, T., Zhang, Z.G., Hayashi, S. and Tomita, A., *Energy & Fuels*, **2**, 1136, (1988).
  25. Carangelo, R.M., Solomon, P.R., and Gerson, D.G., *Fuel*, **66**, 960-967, (1987).
  26. Whelan, J.K., Solomon, P.R., Deshpande, G.V., and Carangelo, R.M., *Energy and Fuels*, **2**, 65, (1988).
  27. Vorres, K.S., "Users Handbook for the Argonne Premium Coal Sample Program", Supported by US DOE, Contract No. W-31-109-ENG-238; (1989).
  28. Bishop, M. and Ward, D.L., *Fuel*, **37**, 191, (1958).
  29. Solomon, P.R., Hamblen, D.G., Carangelo, R.M., Serio, M.A., and Deshpande, G.V., *Energy & Fuels*, **2**, 405, (1988).
  30. Raask, E., *Mineral Impurities in Coal Combustion; Behavior, Problems, and Remedial Measures*, Hemisphere Publishing Corp., NY, (1985).
  31. Solomon, P.R., Chien, P.L., Carangelo, R.M., Best, P.E., and Markham, J.R., *22nd Symposium (Int) on Combustion*, The Combustion Institute, Pittsburgh, PA, 211, (1988).
  32. Solomon, P.R., Best, P.E., Yu, Z.Z., and Deshpande, G.V., *ACS Div. of Fuel Chem. Preprints*, **34**, (3), 895-906, (1989).
  33. Serio, M.A., Solomon, P.R., Kroo, E., Basilakis, R., Malhotra, R., and McMillen, D., "Fundamental Studies of Retrograde Reactions in Direct Liquefaction", Proceedings of the Direct Liquefaction Contractor's Meeting, (Oct. 2-4, 1989).
  34. Khan, M.R., Serio, M.A. Malhotra, R., and Solomon, P.R., *ACS Div. of Fuel Chem. Preprints*, **34**, (4), 1054-1061, (1989).

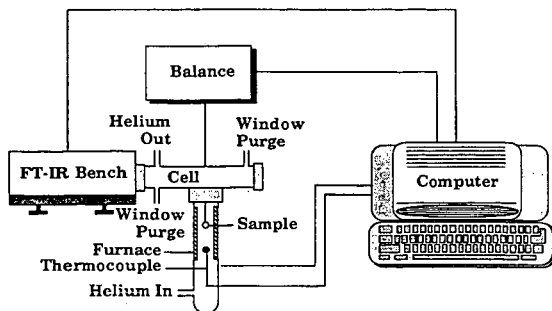


Figure 1. Schematic of TG/plus.

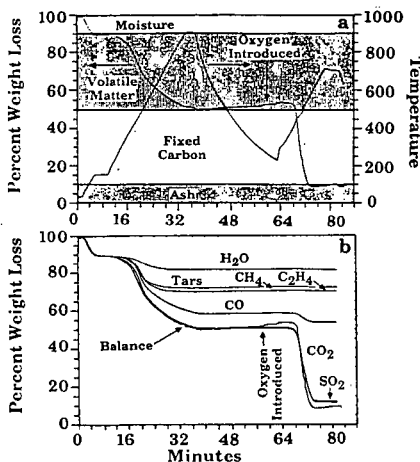


Figure 2. TG-FTIR Analysis of a Lignite. a) Temperature History and Weight Loss. b) Species Contributions to Weight Loss.

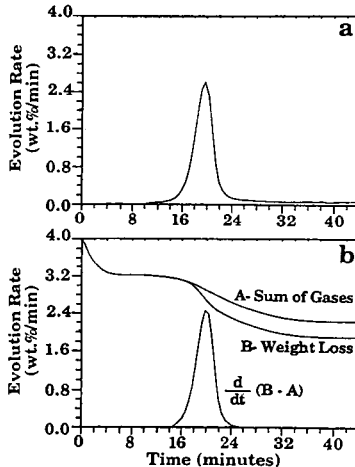


Figure 3. Calibration of Tar Absorptivity. a) Tar Absorption Profile. b) Weight Loss Minus the Sum of Gases.

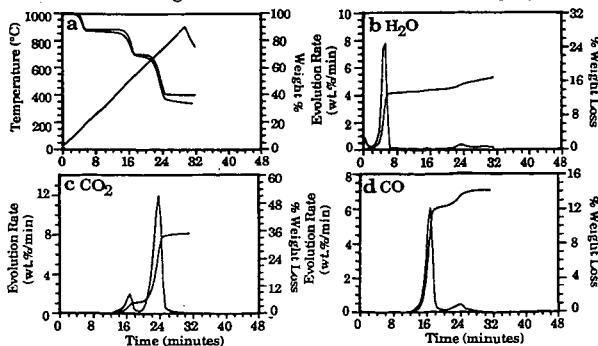


Figure 4. Pyrolysis of Calcium Oxylate. a) Weight Loss (solid), Sum of Evolved Products (dashed), and Temperature Profile. b)  $H_2O$  Evolution, c)  $CO_2$  Evolution, and d)  $CO$  Evolution.

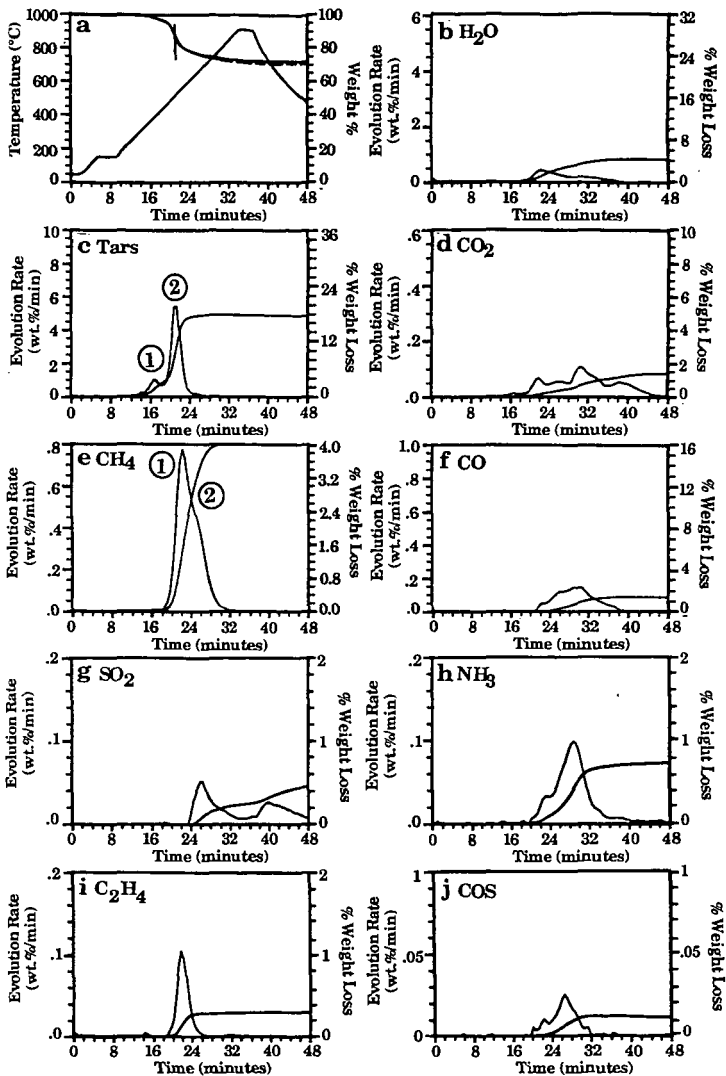


Figure 5. TG-FTIR Analysis of Upper Freeport Bituminous Coal during the Pyrolysis Cycle. a) Weight Loss (solid), Sum of Evolved Products (dashed), and Temperature Profile. b) H<sub>2</sub>O Evolution Rate and Integrated Amounts Evolved, c) Tar Evolution Rate and Integrated Amounts Evolved, d) CO<sub>2</sub> Evolution Rate and Integrated Amounts Evolved, e) Methane Evolution Rate and Integrated Amounts Evolved, f) CO Evolution Rate and Integrated Amounts Evolved, g) SO<sub>2</sub> Evolution Rate and Integrated Amounts Evolved, h) NH<sub>3</sub> Evolution Rate and Integrated Amounts Evolved, i) C<sub>2</sub>H<sub>4</sub> Evolution Rate and Integrated Amounts Evolved, and j) COS Evolution Rate and Integrated Amounts Evolved.

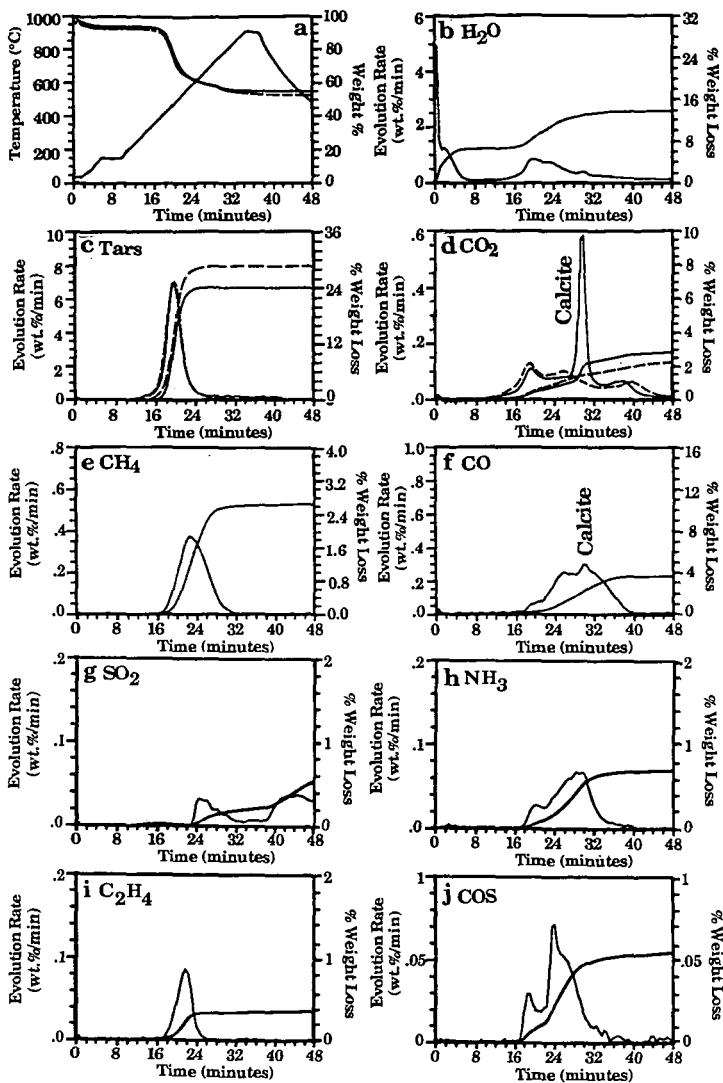


Figure 6. TG-FTIR Analysis of Illinois No. 6 Bituminous Coal during the Pyrolysis Cycle. a) Weight Loss (solid), Sum of Evolved Products (dashed), and Temperature Profile. b) H<sub>2</sub>O Evolution Rate and Integrated Amounts Evolved, c) Tar Evolution Rate and Integrated Amounts Evolved (raw coal (solid line) demineralized coal (dashed line)), d) CO<sub>2</sub> Evolution Rate and Integrated Amounts Evolved (raw coal (solid line) demineralized coal (dashed line)), e) Methane Evolution Rate and Integrated Amounts Evolved, f) CO Evolution Rate and Integrated Amounts Evolved, g) SO<sub>2</sub> Evolution Rate and Integrated Amounts Evolved, h) NH<sub>3</sub> Evolution Rate and Integrated Amounts Evolved, i) C<sub>2</sub>H<sub>4</sub> Evolution Rate and Integrated Amounts Evolved, and j) COS Evolution Rate and Integrated Amounts Evolved.

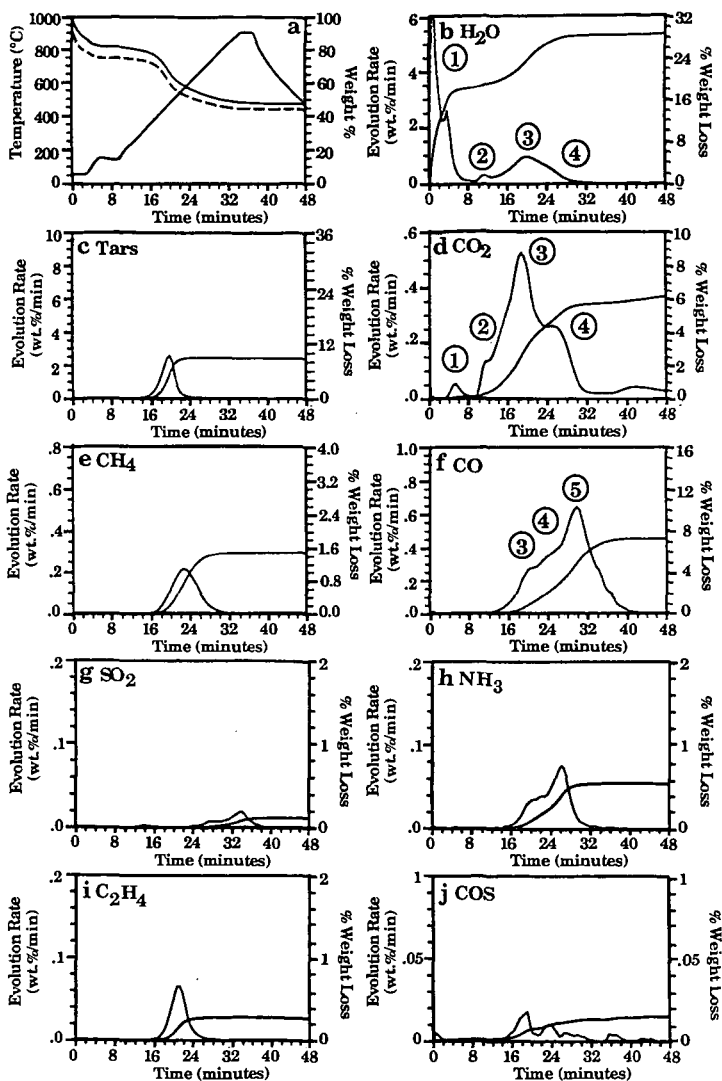


Figure 7. TG-FTIR Analysis of Wyodak Subbituminous Coal during the Pyrolysis Cycle. a) Weight Loss (solid), Sum of Evolved Products (dashed), and Temperature Profile. b) H<sub>2</sub>O Evolution Rate and Integrated Amounts Evolved, c) Tar Evolution Rate and Integrated Amounts Evolved, d) CO<sub>2</sub> Evolution Rate and Integrated Amounts Evolved, e) Methane Evolution Rate and Integrated Amounts Evolved, f) CO Evolution Rate and Integrated Amounts Evolved, g) SO<sub>2</sub> Evolution Rate and Integrated Amounts Evolved, h) NH<sub>3</sub> Evolution Rate and Integrated Amounts Evolved, i) C<sub>2</sub>H<sub>4</sub> Evolution Rate and Integrated Amounts Evolved, and j) COS Evolution Rate and Integrated Amounts Evolved.

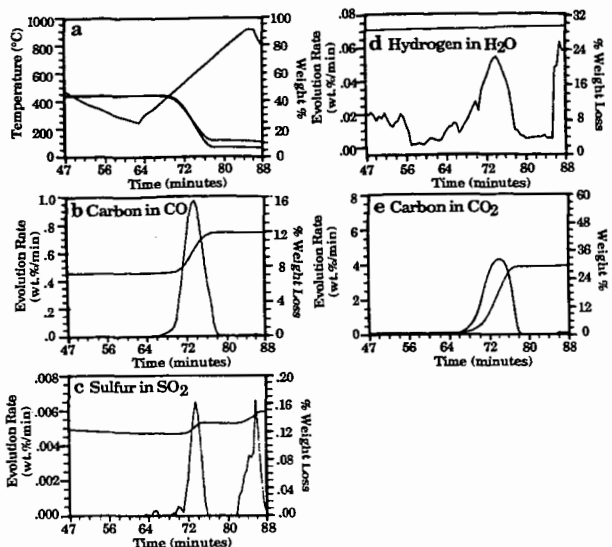


Figure 8. TG-FTIR Analysis of Wyodak Subbituminous during the Combustion Cycle. a) Weight Loss (solid), Sum of Evolved Products (dashed), and Temperature Profile. b) Carbon in CO Evolution Rate and Integrated Amount Evolved. c) Sulfur in SO<sub>2</sub> Evolution Rate and Integrated Amount Evolved. d) Hydrogen in H<sub>2</sub>O Evolution Rate and Integrated Amount Evolved. e) Carbon in CO<sub>2</sub> Evolution Rate and Integrated Amount Evolved.

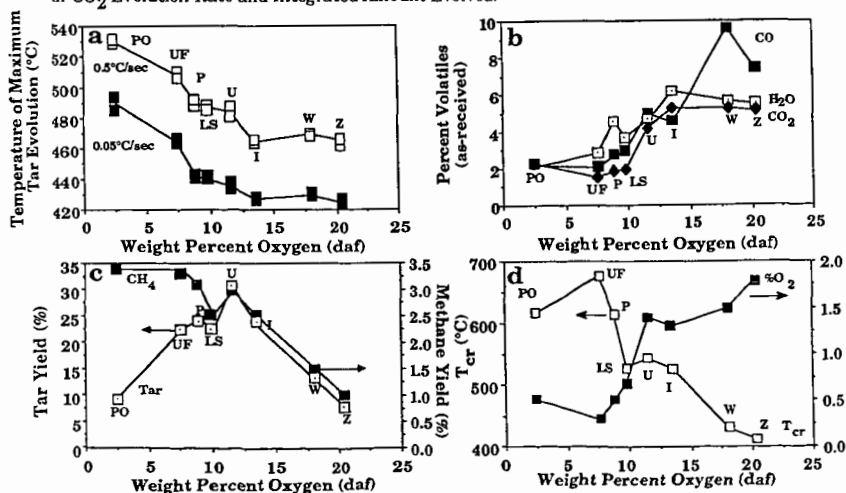


Figure 9. Variation of Coal Pyrolysis Properties with Rank. a) Rank Variation of Tar Evolution Temperature, b) Rank Variation of Oxygenated Gases c) Rank Variation of CH<sub>4</sub> and Hydrocarbons and d) Rank Variation of T<sub>cr</sub> and Oxygen Chemisorption.